Supplement of Atmos. Meas. Tech., 8, 2121–2148, 2015
http://www.atmos-meas-tech.net/8/2121/2015/
doi:10.5194/amt-8-2121-2015-supplement

Atmospheric Measurement Techniques
Open Access

Supplement of

Aircraft measurements of BrO, IO, glyoxal, NO_2, H_2O, O_2–O_2 and aerosol extinction profiles in the tropics: comparison with aircraft-/ship-based in situ and lidar measurements

R. Volkamer et al.

Correspondence to: R. Volkamer (rainer.volkamer@colorado.edu)

Supplementary Information

Spatial scales

The spatial scale sampled by CU AMAX-DOAS, defined as the sum of translational movement of the aircraft and the extinction length of photons, corresponds to about 35 km at ultraviolet wavelengths (BrO), and 100 km at visible wavelengths (IO and glyoxal) in the FT. This volume of air is sampled near instantaneously from the aircraft, and closely resembles the spatial scales represented in atmospheric models (~30 km for WRF; ~15 km for RAQMS in RDF mode), satellite footprints (~13x24 km^2 for OMI; ~30x60 km^2 for SCIAMACHY; ~40x80 km^2 for GOME-2), global models (~60 km for GEOS-Chem; ~110 km for CAM-Chem, WACCM, TM4-ECPL; ~300 km for RAQMS in forecast mode), spatial scales of Deep Convective Cloud features (~50-300 km), and cirrus clouds (up to 1000 km).

Sensitivity study – tropospheric BrO

We have conducted a sensitivity study to test the effect of a sharp gradient in BrO right above the tropopause (Salawitch et al., 2005) on the tropospheric BrO profile retrieved from limb-observations. The sensitivity study placed (unrealistic) 20pptv BrO in a layer between 17 and 18 km (we assume 4pptv between 14 and 17 km). The profile inversion responds with less than 0.18 pptv additional BrO at 13.7 km, which is insignificant within the inversion error bars. This confirms that our limb measurements are insensitive to stratospheric BrO even for extreme concentration gradients.

BrO in the UTLS: Method context

Much of the current knowledge of BrO chemistry in the UTLS is based on balloon-borne direct-sun measurements (Pundt et al., 2002; Dorf et al., 2008). Some balloon-borne direct sunlight DOAS measurements have reported tropospheric BrO levels in reasonable agreement with GOME at extra tropical latitudes (Fitzenberger et al., 2000; Van Roozendael et al., 2002). In the tropics, however, only very limited balloon-borne tropospheric BrO profiles are available (Dorf et al., 2008), and these profiles have detected about an order of magnitude less BrO (<1 pptv) in the troposphere than reported in this study, and previous column observations (Chance, 1998;

Fitzenberger et al., 2000; Wagner et al., 2001; Richter et al., 2002; Van Roozendael et al., 2002; Salawitch et al., 2005; Hendrick et al., 2007; Theys et al., 2007; Coburn et al., 2011; Theys et al., 2011). The reasons for the difference are currently not clear, and could be attributable to atmospheric variability.

Direct-sun observations have been very successfully applied for profiling in the stratosphere. A direct comparison of the information content for tropospheric BrO with our data is complicated by the fact that there is no mentioning about the DoF, or AVK in the peer-reviewed literature regarding BrO direct-sun observations (Pundt et al., 2002; Dorf et al., 2008). The one BrO profile inversion where this information is available is from Kiruna, Sweden (Dorf, M., 2005, Investigation of Inorganic Stratospheric Bromine using Balloon-Borne DOAS Measurements and Model Simulations, PhD thesis, University of Heidelberg, Germany). That profile showed ~1 DoF and AVK that peak around 0.1-0.2 in the troposphere (below 8 km), and 12 DoF in the stratosphere. At tropical latitudes the SZA changes faster than at high latitudes (about 4 times faster over the course of a balloon ascent), which makes decoupling tropospheric from stratospheric BrO less straightforward in the tropics.

Limb measurements are possible over a wider range of SZA. Measurements at very small SZA (e.g., near overhead sun) inherently minimize the contribution of stratospheric BrO, and facilitate a straightforward and robust correction of stratospheric BrO (see "Quality of stratospheric correction" in Section 3.2.1) also at tropical latitudes (Sect. 4.2., Fig. 10). The limb geometry is optimized towards locating BrO in the troposphere, and decoupling stratospheric BrO (see below "Sensitivity study – tropospheric BrO"). Further, the instrument sensitivity peaks at instrument altitude (see Box-AMFs, Fig. S2), and measurements from aircraft facilitate excellent altitude control. Our limb observations have 12-13 DoF to characterize tropospheric BrO (Fig. 7). A higher number of DoF is in principle possible from higher time resolved BrO observations over an altitude range similar to RF12. More BrO profiles are needed to test whether the findings of high BrO apply more broadly in the tropics.

Further sensitivity studies for IO

Sensitivity tests on DOAS analysis settings showed a slight sensitivity of IO dSCDs towards the choice of polynomial degree (~25% higher dSCDs for a 4^{th} order polynomial), but dSCDs were robust towards variations in the fit window. The starting wavelength of the fit window has been moved from 415 to 417 nm, compared to Dix et al. (2013), because the HITRAN 2008 H_2O cross section has been replaced by a spectrum from HITEMP 2012 for the TORERO analysis. HITEMP includes more and stronger absorption lines between 410 and 438 nm and a more distinct absorption peak at ~416.5 nm that is now excluded from the TORERO IO analysis. The results from a sensitivity test where the HITEMP H_2O reference spectrum (Table 1) was substituted for a HITRAN H_2O spectrum show 16% higher IO dSCDs compared to using the HITEMP spectrum (see Fig. S3), while the offset remained zero within error ($0.5\pm1.0\times10^{12}$ molec cm^{-2}). One further change compared to Dix at al., 2013 is that we are not fitting an additional residual cross section for IO anymore. Similar to (Schonhardt et al., 2008; Schonhardt et al., 2012), who present satellite IO measurements, we observe a systematic residual structure around 432 nm that is likely caused by an improperly corrected Fraunhofer line. While Schoenhardt et al. analyze IO from 416-430 nm to avoid this wavelength region, the analysis of all TORERO RFs has shown that this particular Fraunhofer line does not significantly affect our fit stability, nor RMS. Fitting an additional residual cross section is not necessary.

Assessment of SCD_{REF} for IO

For IO the value of SCD_{REF} is likely non-zero, and the reference geometries have limited flexibility to inherently minimize SCD_{REF} for IO retrievals (see Sect. 2.8). This is different for IO than for the other gases, where SCD_{REF} can be systematically minimized (e.g., zero for glyoxal), or kept constant within negligible error (e.g., BrO and NO_2, see Sects. 3.2.2. and 4.2.). What is unique for IO is that the MBL EA0 geometry maximizes SCD_{REF} due to the IO profile shape, and the MBL EA+90 leads to higher RMS for reasons that are currently unknown. We use an EA0 spectrum from RF12 for our analysis of both RF12 and RF17 flights; this does not present a fundamental problem, since the IO dSCDs from comparing EA0 references at different altitudes leads to a consistent offset that can be understood from the IO profile (Sect. 3.2.1.). However,

this might complicate the correction of small amounts of IO that may reside in the lower stratosphere (Wennberg et al., 1997), as is illustrated by the shape of Box-AMFs in Fig. 6A. Assuming 0.1ppt IO between 17 and 45 km, and no IO throughout the troposphere, we estimate that the SCD_{REF} for RF12 is 0.66 x10^{12} molec cm^{-2} IO for EA0 at 14.5 km, and 0.64 x10^{12} molec cm^{-2} IO for EA+10 at 14.5 km. Our limb-measurements at 14.5 km are essentially insensitive to such small amounts of stratospheric IO. Also, the insignificant change for different viewing geometries suggests that stratospheric IO, if present, cancels well (error few percent). We thus assume our measured IO dSCDs to be representative of IO SCDs, and use these in the inversion of IO, as discussed in Sect. 2.8.

H_2O spectral line parameters and glyoxal retrievals

We prefer using the HITEMP H_2O cross section over HITRAN in our final analysis, because laboratory tests to measure H_2O absorption spectra using CE-DOAS at blue wavelengths at CU Boulder more closely resemble the HITEMP than the HITRAN spectra (Coburn et al., 2014). The most prominent unaccounted H_2O features were observed are between 441 and 447 nm, and the strongest peak is near 442nm. All of these bands are shifted and well separated from the strongest glyoxal bands near 455nm. H_2O features in the range of 450 to 458 nm are 10-20 times weaker than the 442nm peak, and unaccounted H_2O features in this spectral range could have optical densities on the order of ~1-2 10^{-4} for H_2O SCDs of 7.3 x10^{23} molec cm^{-2}. Our laboratory measurements confirm that high-resolution water cross-section measurements are desirable. They also suggest that the quality of water correction is best indicated near 442 nm.

Figure S3 shows dSCDs evaluated using identical analysis settings (Table 1), but using either a HITEMP (Rothman et al., 2010) or HITRAN (Rothman et al., 2013) H_2O cross section spectrum for analysis of RF17. The difference in the glyoxal dSCD is about 10%, and no significant offset is observed (< 0.1±0.3×10^{14} molec cm^{-2}). We see no noticeable difference (error within 2%) if a water reference, or water residual is used during spectral fitting of glyoxal dSCDs (Sinreich et al., 2010). The glyoxal dSCDs further did not change significantly (error within 5%) whether the residual is included or not (Fig. S3). With either HITEMP or HITRAN cross-sections the fit finds a consistent solution if the residual is added to the water cross-section (difference between

slopes of 1.06 and 1.04, see Fig. S3). As an extreme test, if the HITEMP residuum is fitted with the HITRAN cross-section, the slope in Fig. S3 increases to 1.13, but the offset remains negligible (not shown). Sensitivity tests showed no significant correlation between glyoxal and H_2O dSCDs (< 0.05 for 3rd to 5th order). The 5th order polynomial for AMAX showed the lowest degree of correlation, and is the polynomial order chosen for our AMAX analysis.

Recently, Thalman et al. (2014a) tested the sensitivity of glyoxal retrievals on water under simulated atmospheric conditions, as part of an intercomparison campaign where seven different techniques to measure glyoxal, including CE-DOAS participated. We did not find any noticeable sensitivity for glyoxal SCDs in DOAS retrievals of spectra recorded in dry and moist air (tested up to 58% RH). The glyoxal concentrations were generally higher in that study (~200 pptv), but the CE-DOAS sensitivity was suitable to assess changes in glyoxal of atmospheric relevance. Recent EC flux measurements of water and glyoxal during the TORERO cruise further showed no evidence for an obvious sensitivity at ~30 pptv glyoxal at 80% RH (Coburn et al., 2014). While the water fluxes were consistently positive (indicating evaporation), the glyoxal fluxes were positive at night, and more positive in certain parts of the ocean, but negative during most of the daytime. The H_2O and glyoxal EC fluxes showed no evidence of a correlation.

Note on H_2O measurements

The rather weak H_2O cross-section at 442 nm has good signal-to-noise to detect water below 9 km, but dSCDs are close to the noise level at higher altitudes. As indicated in Fig. 7, the AMAX-H_2O AVKs peak near unity at and below 9 km, and rapidly decrease at higher altitudes. There is room to improve signal-to-noise for AMAX-H_2O, probably by a factor 10-20, if stronger H_2O cross-sections at longer wavelengths are used (e.g., 510 nm), which has the further benefit of longer absorption paths. No attempts have been made to optimize the AMAX-H_2O retrievals in this respect, and we limit the discussion of AMAX-H_2O profiles to altitudes below 9 km; data at higher altitudes should be viewed as qualitative.

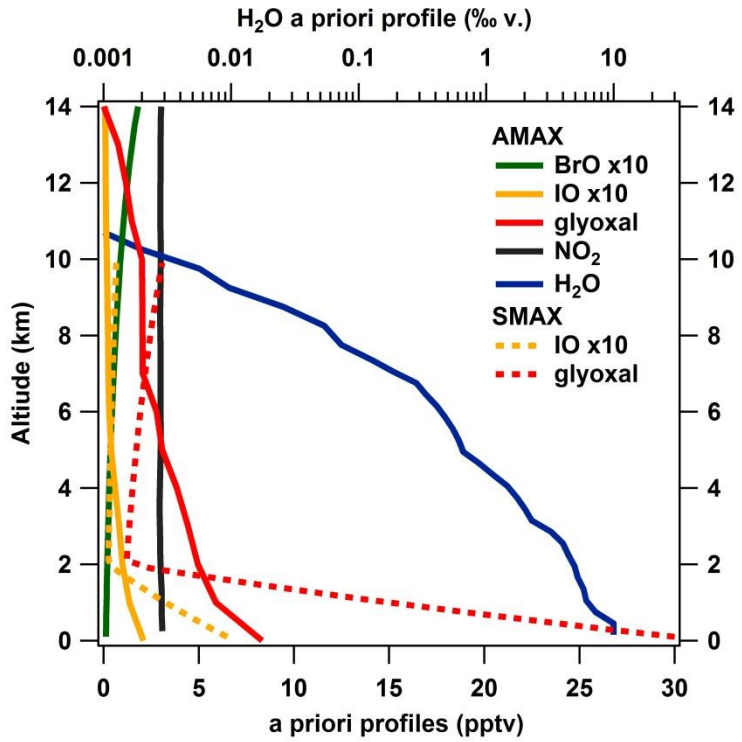

Figure S1: *A priori profiles used in the Optimal Estimation retrievals of AMAX and SMAX DOAS data.*

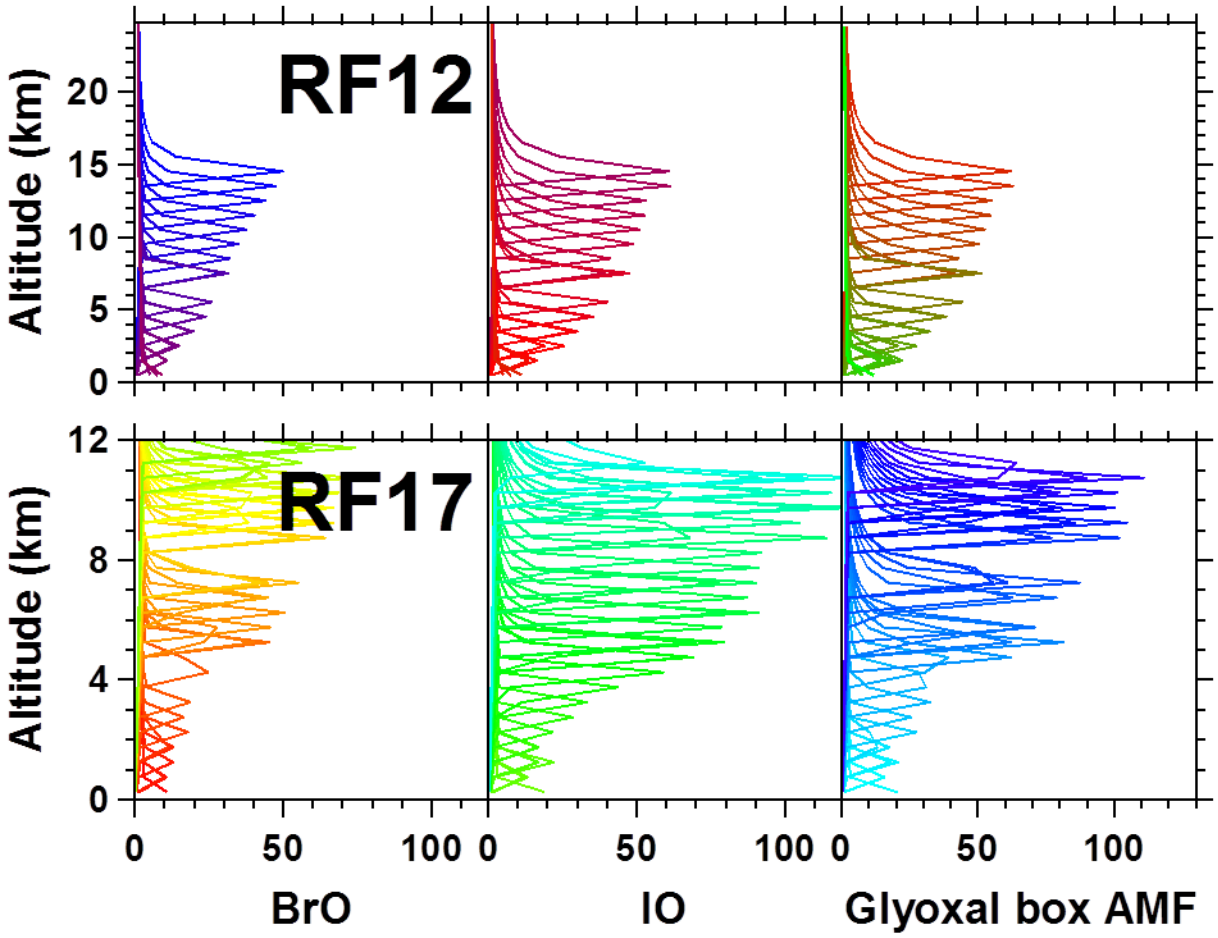

Figure S2: *Box-AMFs calculated at 350nm (BrO), 428nm (IO) and 450nm (Glyoxal) using the respective aerosol profiles for the RF12 and RF17 profile case studies.*

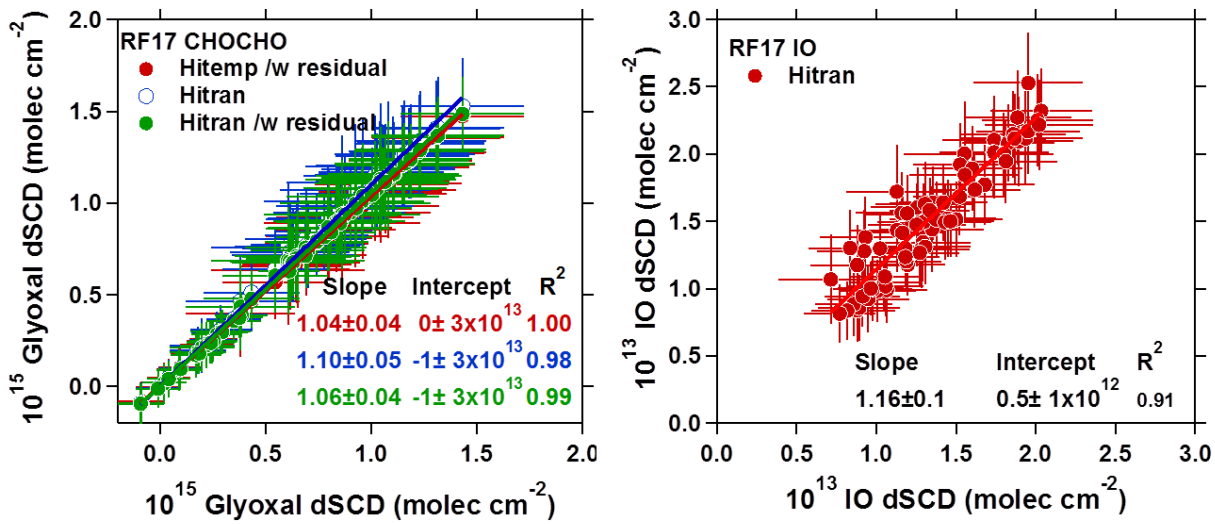

Figure S3: *Sensitivity studies to explore changes in glyoxal and IO dSCDs towards uncertainties in the water cross-section.*

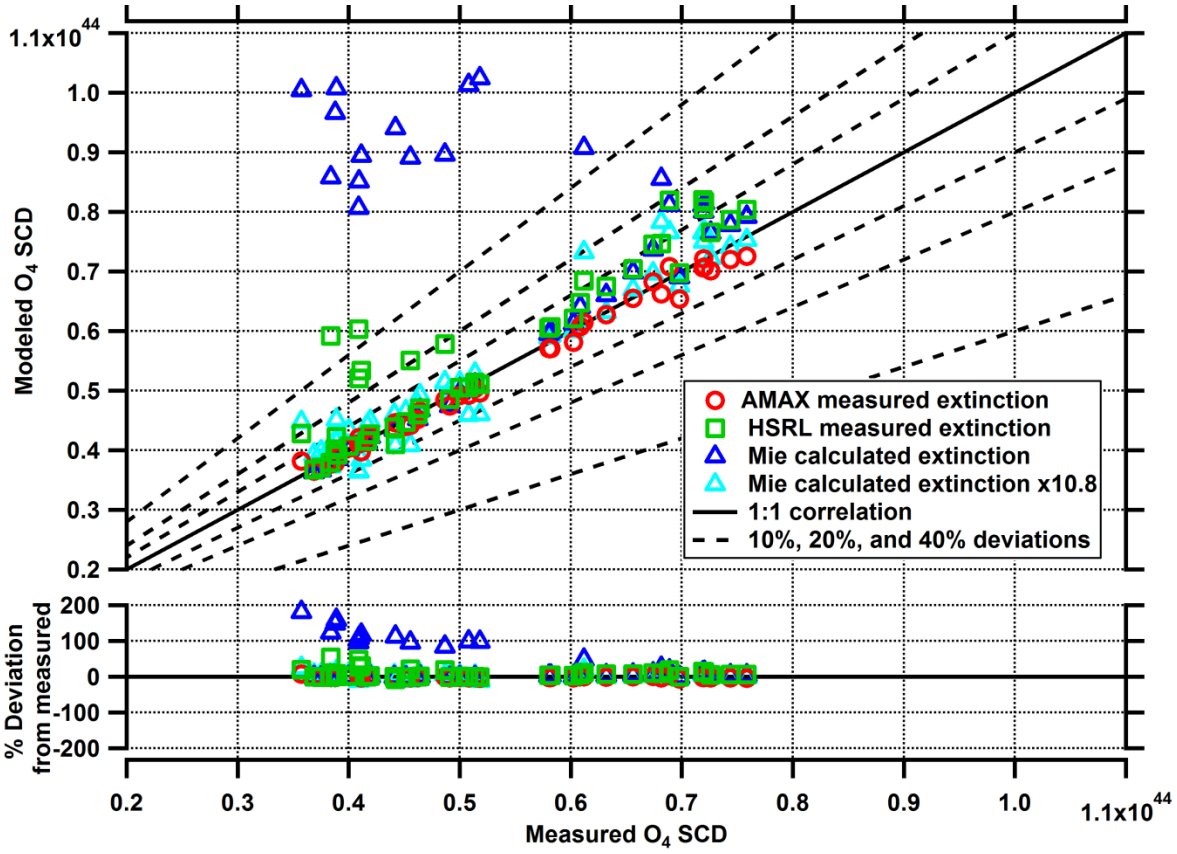

Figure S4: *Comparison of measured and predicted O_4 SCDs for the RF17 case study, using the HSRL, UHSAS, and scaled UHSAS aerosol extinction. The lower panels show the relative difference to the 1:1 line; the average difference and standard deviation for O_4 was (-1 ±1) % and (+8±13) % for HSRL in the lower 400m, and over the full altitude range, respectively; for UHSAS: (+99±1) % and (+40±50) %; and for UHSAS x 10.8: (-10±1) % and (+3±8) %.*